Modification on theory of sink strength: an Object Kinetic Monte Carlo study

Jie Hou[a,b], Xiang-Shan Kong[a], Xiang-Yan Li[a], Xuebang Wu[a,*], C. S. Liu[a,*], Jun-Ling Chen[c], G.-N. Luo[c]

[a] *Key Laboratory of Materials Physics, Institute of Solid State Physics, Chinese Academy of Sciences, Hefei 230031, P. R. China*

[b] *University of Science and Technology of China, Hefei 230026, P. R. China*

[c] *Institute of Plasma Physics, Chinese Academy of Sciences, Hefei 230031, P. R. China*

Abstract

Sink strength is a fundamental quantity in modeling the microstructure evolution of irradiated materials by the mean-field approaches. The analytical expressions for different sinks have been extensively studied. The Object Kinetic Monte Carlo (OKMC) simulations were subsequently performed to corroborate the expressions and to guide the development of analytical theories. Although a general agreement was found between the theory and simulation, there are still some discrepancies in the case of the small spherical sinks and the dislocation lines. In this work, OKMC simulations were performed to study the sink strength of spherical sinks and dislocation lines. Our results revealed the origins of discrepancies between the theory and simulation for small sinks, high volume fraction sinks and periodically distributed dislocation lines. The theoretical corrections were also proposed accordingly. These corrections can extend the capabilities of mean-field approaches to properly reproduce the defect evolution of irradiated materials, and provide a better insight into the experimental phenomena, such as the defect cluster nucleation, the irradiation-induced swelling and the blistering.

[0]*Authors to whom correspondence should be addressed. Tel: 0086-551-65591062 E-mail address: csliu@issp.ac.cn(C. S. Liu), xbwu@issp.ac.cn(X. B. Wu)

1. Introduction

The degradation of material properties under irradiation is a main concern in reactor design. Under the high-energy particle irradiation, numerous mobile defects such as interstitials and vacancies are created. The clustering and aggregation of these defect are generally relevant to the the formation of blisters and voids, which leads to the degradation of materials. These mobile defects can interact with each other and with other sinks such as grain boundaries and dislocation lines. The ability of these sinks to capture the migrating defects can be quantitatively described by the sink strength that was applied in mean-field approaches for simulations of defect evolution.

The sink strength is proportional to the inverse square of average free migration distance of defects. It is connected to the size, shape and density of sinks, as well as the dimensionality of defect migration, i.e., three-dimensional (3D), one-dimensional (1D), or mixed 3D/1D. Based on the diffusion theory, many theoretical work has been carried out to obtain the analytical sink strength for different sinks. Brailsford and Bullough et al. have investigated the expressions for the spherical sinks [1] and grain boundaries [2] under the 3D limit. Similar expression for dislocations was derived by Wiedersich [3], corrected by Nichols [4], and shows a good agreement with the phase-field results [5]. Theoretical sink strengths for these sinks under the 1D limit were systematically investigated by Barashev et al. [6]. Recently, the Object Kinetic Monte Carlo (OKMC) method [7–9] which is expected to provide the sink strengths spontaneously, has been used to corroborate these expressions and to guide the development of the theories. The OKMC simulations by Malerba and Jansson et al. [10, 11] showed good agreements with analytical theory in both the 3D and 1D limits, as well as in the transition regime of 3D to 1D diffusion. The transition region is described by a single-variable

function (master-curve), which was proposed by Trinkaus and Heinisch et al. and also confirmed by the OKMC simulations [12–15].

Despite of the general agreements found between theoretical works and simulations, unexplained discrepancies under certain situations have also been found in previous studies. More specifically, the OKMC simulation results always show an underestimate of the analytical sink strength for small sinks [10, 13, 16], and a huge overestimate for high volume fraction sinks [10, 11, 13]. An irregular discrepancy for periodically distributed dislocation lines was also pointed out[11]. Heinisch et al. [13] attributed the underestimation to different nature between the diffusion mechanisms in OKMC and theoretical model. They thereby provided a fitted correction term, which works well for the sink radii above $2.5a_0$ (a_0 is the lattice constant). However, they did not consider the effectiveness of the correction for the smaller sink ($< 2.5a_0$, such as vacancy clusters containing about 100 vacancies). More importantly, the corrected expression cannot describe point defects like mono-vacancy because it predicts a zero sink strength. Since OKMC is *a priori* expected to provide the same sink strength to that provided by the diffusion theory, additional corrections should be required for OKMC or mean-field simulations of defect cluster nucleation.

In this work, we calculated sink strengths of different sinks through both the theoretical and OKMC approaches, for the defects characterized by a varying motion dimensionality from the fully 3D limit to the pure 1D limit. Particular cares were taken for the small sinks, the high volume fraction sinks and the dislocation lines in the 1D migration limit. The theoretical corrections thereof were also provided to eliminate the discrepancies mentioned above. It was found that much better agreements between theory and simulation can be achieved after the corrections.

2. Computation method

An OKMC program is designed to calculate sink strengths of spherical sinks and dislocation lines. The entire procedure is similar to that used in refs. [10, 11]. Briefly, defects and sinks are treated as objects with specific positions in a simulation box and with associated reaction volumes. Probability of a thermally activated event, such as defect migration, is given in the form of Arrhenius frequency, $\Gamma_i = \upsilon_i exp(-E_{a,i}/k_B T)$. Here υ_i is the attempt frequency for event i, $E_{a,i}$ is the corresponding activation energy, k_B is the Boltzmann constant, and T is the absolute temperature. An event is randomly chosen according to its probability. The binary search algorithm is applied here to accelerate the choosing procedure. After the event is executed, the object configuration will be updated, and the simulated time will be increased according to the resident time algorithm [17], $\Delta\tau = 1/(\Sigma_{i=1}^{N_{int}}\Gamma_i^{int} + \Sigma_{j=1}^{N_{ext}}\Gamma_j^{ext})$, where N_{int} and N_{ext} are the number of internal and external events, respectively. Here, two internal events are considered, including defect migration and rotation of migration direction. No external events are considered in this work, i.e., $N_{ext} = 0$. Note that, when two objects overlap geometrically, reactions between these two defects will take place. For instance, absorptions of a point defect take place when its distance to a sink is smaller than the sum of their capture radii. This kind of event will bring no time increment to the system. During the simulation, events are chosen and executed repeatedly until certain time or steps are achieved. In this work, in order to achieve a statistical convergence, simulations will not be stopped until 10000 point defects are absorbed.

Similar to previous works[10, 13, 14], a model handles only idealised situations is implemented. In this model, a point defect with zero radius is introduced at a random position and allowed to migrate. After its absorp-

tion, a new point defect will be introduced instantaneously so that only one point defect at a time is presented in the system. It should be pointed out that defects created inside spherical sinks or dislocation lines are not taken into account. In this way, the sink strength, k^2, can be given by:

$$k^2 = \frac{2n}{d^2 < m >}, \tag{1}$$

where n is the dimensionality of point defect migration, which is taken as 3 even for 1D migrating in order to consistently trace the transition between 1D and 3D migration. d is the migration distance of a point defect, which equals $\sqrt{3}a_0/2$ in bcc tungsten with lattice constant $a_0 = 0.3165$ nm. $< m >$ is the average number of jumps before it is absorbed by sinks. Similar to ref. [10], the dimensionality of defect motion is changed by assigning a rotation energy E_r to defects, whereby the probability of changing migration direction is expressed as $\exp(-E_r/k_BT)$. One can set $E_r = 0$ to acquire pure 3D migration or set E_r to a relatively high value to get pure 1D migration (<111> directions in tungsten). In this work, at the chosen simulation temperature of 723 K, $E_r = 1.5$ eV is enough to provide a fully 1D path, while the intermediate values are considered to give a mixed 1D/3D migration.

A non-cubic periodic box with a fixed size ratio $l_x : l_y : l_z = \frac{1}{\sqrt[4]{2}} : \sqrt[4]{2} : 1$ is employed in order to correctively describe the 1D migrating of point defects [10]. The irrational ratio of box sides was used to ensure that any super-box of this box would be non-cubic. Spherical sinks are randomly introduced in this non-cubic box with $l_z = 350$ nm. The radius of spherical sinks, R_s, varied from 0.27 to 10.25 nm. And their number density, N_s, varied from 10^{-5} to 1.5×10^{-4} nm^{-3} for the 3D and 1D migration. For the mixed 1D/3D migration, a fixed $R_s = 4.25$ nm was used and N_s varied from 3×10^{-5} to 1.5×10^{-4} nm^{-3}. As shown in Fig. 1, the dislocation line is introduced as a cylindrical sink whose two opposite faces touch the faces of

the simulation box. Only one dislocation line is introduced along l_z direction of the simulation box. However, under the periodic boundary condition, this model is practically equivalent to a regular array of infinitely long dislocation lines. Different surface densities can be obtained by changing the box size. Here, l_z varied from 15 to 45 nm while keep the size ratio fixed, corresponding to surface densities from 5×10^{-4} to 4.5×10^{-3} nm^{-2}. The dislocation radius used here, R_d, varied from 0.25 to 10 nm. Some large R_d are not used for small boxes due to the box size limit, and some small ones are not used for large boxes owing to the computational time limit.

3. Results and discussion

3.1. Spherical sinks

3.1.1. Results without any correction

The analytical sink strength of spherical sinks under 3D migration limit is given by [1]:

$$k_{3,s}^2 = 4\pi R_s N_s (1 + k_{3,s} R_s). \tag{2}$$

This equation is usually solved by the iterative method. The n^{th} order of iterative result is calculated by $k_{3,s,n}^2 = 4\pi R_s N_s (1 + k_{3,s,n-1} R_s)$, with the first order given as $k_{3,s,1}^2 = 4\pi R_s N_s$. As proposed by previous work [10], it is necessary to use high orders of iterative approximation for a good agreement between the theoretical expression and the OKMC simulation. For Eq. (2), the larger the R_s is, the poorer the convergence will be. Even so, as shown in Fig. 2, for the largest $R_s = 10.25$ nm used in this work, a good convergence is already achieved at the third order approximation. In this work, the fifth order approximation is adopted for all calculations using Eq. (2), and for similar equation Eq. (4). In the case of 1D migrating defects, expression of

the sink strength is given by [6]:

$$k_{1,s}^2 = 6(\pi R_s^2 N_s)^2. \tag{3}$$

In our OKMC simulations, spherical sinks were introduced randomly but without overlap with each other. Under the 3D migration limit, the radius of spherical sink, R_s, varied from 0.27 to 10.25 nm (0.27, 0.75, 1.25, 2.25, 4.25, 6.25, 8.25, and 10.25 nm), and their number density, N_s, varied from 3×10^{-5} to 15×10^{-5}nm^{-3} (1.0, 3.0, 6.0, 9.0, 1.2, and 15.0×10^{-5}nm^{-3}). The two highest densities were not considered when $R_s = 10.25$ nm, because of the limitation of non-overlap. For the 1D migration limit, it is impossible to produce all the data points explored in the 3D case owing to computational time reasons. The same densities to the 3D case are all taken into account for $R_s > 4.25$ nm. While only one number density ($N_s = 10^{-3}$ nm^{-3}) is considered when $R_s < 4.25$ nm (0.75, 1.25, 1.75, 2.25, 2.75, 3.25 and 3.75 nm).

Fig. 3 presents results of sink strength under the 3D and 1D migration limits. Similar to previous studies [10, 13], a general agreement is found between analytical theory and simulation. Whereas two significant discrepancies can also be identified for small sinks under the 3D limit and for the high volume fraction sinks. These discrepancies can be clearly displayed by relative errors, defined as the percentage ratio of simulated-analytical sink strength difference to analytical sink strength, i.e., $(k_{sim}^2 - k_{ana}^2)/k_{ana}^2 \times 100\%$. As shown in Fig. 4(a), the simulated sink strength is about 33% lower than the analytical one for the smallest sink under the 3D migration limit. Meanwhile, errors for the same sink radius are close. This indicates that the sink radius is the key variable of such errors. However, for the 1D limit that shown in Fig. 4(b), similar errors for small sinks are not observed. With the growing of sink radius, in the volume fraction range of $10^{-4} \sim 10^{-1}$, the

relative error reduces to nearly zero in both cases, suggesting a good agreement between theoretical works and simulations. When the volume fraction is above 10^{-1}, the relative error grows very rapidly with the increase of sink volume fraction. This implies a large discrepancy between theory and simulation data. In order to eliminate the discrepancies, further investigations and additional corrections are required.

3.1.2. Correction for small sinks

The discrepancy for small sinks under the 3D migration limit is often attributed to different nature of diffusion mechanisms between the theory and the OKMC simulation [13, 16]. As shown in Fig. 5(a). For the theoretical model, the diffusion is a continuous process, where point defects are absorbed exactly at the sink surface. For the OKMC simulation, the diffusion is a discrete process composed of a series of individual hops, where the absorption takes place when a defect jumps into the sink. Since the jump distance d is not zero, point defects in OKMC simulation can penetrate into the sink. The penetration area is not an ideal spherical surface but a spherical shell (gray area in Fig. 5(a)). Therefore, R_s in the Eq. (2) should be revised by adding a correction term ΔR:

$$k_{3,s}^2 = 4\pi(R_s + \Delta R)N_s[1 + k_{3,s}(R_s + \Delta R)]. \tag{4}$$

Here, $R_s + \Delta R$, is denoted by R_{eff}, namely the effective radius of the sink.

For the 3D limit, the thickness of the penetration area in the OKMC model is the jump distance d. Since the sink strength of spherical sinks varies linearly with the radius for small sinks, the correction term ΔR should be weighted average of the penetration depth p:

$$\Delta R = -\overline{p} = \overline{r - R_s}, \tag{5}$$

where $r = R_s - p$ is the distance to sink center. For a certain r, its possible start point (red dot) of the last jump falls on a spherical cap surface with radius d centered at destination point (black dot). Form r to $r + \mathrm{d}r$, the possible start point is given by shifting the spherical cap surface by $\mathrm{d}r$ (shadow area in Fig. 5(a)). The volume of this area is given by the differential of spherical cap volume[18]:

$$\mathrm{d}V = \pi \frac{d^4 + (r^2 - R_s^2)^2 - 2d^2(r^2 + R_s^2)}{4r^2} \mathrm{d}r. \tag{6}$$

The correction term is given by:

$$\Delta R = \overline{r - R_s} = \frac{\int_{R_s - d}^{R_s} (r - R_s) 4\pi r^2 \frac{\mathrm{d}V}{\mathrm{d}r} \mathrm{d}r}{\int_{R_s - d}^{R_s} 4\pi r^2 \frac{\mathrm{d}V}{\mathrm{d}r} \mathrm{d}r}, \tag{7}$$

where $4\pi r^2 \frac{\mathrm{d}V}{\mathrm{d}r} \mathrm{d}r$ represents the set of start points that can jump to a spherical shell between r and $r + \mathrm{d}r$, namely, the weight of r. Substituting Eq. (6) into Eq. (7), we have:

$$\Delta R = -\frac{5d^2 + 16dR_s - 30R_s^2}{16d^2 + 30dR_s - 80R_s^2} d. \tag{8}$$

By substituting this correction term into Eq. (4), we calculated percentage errors after the effective radius correction. The modified sink strength and its corresponding relative error are calculated and summarized in Fig. 6. It clearly shows that that discrepancies for small sinks are perfectly removed after the effective radius correction.

We also noticed that there is no discrepancy for small sinks under 1D limit. This can be understood as follows. As shown in Fig. 5(b), under 1D migration limit, the sink strength is connected to the biggest cross-section of the sink perpendicular to the migration direction. Under the continuous diffusion mechanism, point defects are absorbed exactly at the sink surface. Therefore, the radius of the biggest cross-section is equal to the sink radius

R_s. While in the OKMC simulation, as stated before, point defects can penetrate into the sink. The penetration area here is the gray area between the two spherical surfaces separated by d in the migration direction. R_{eff} is thereby given by the radius of the biggest cross-section of the penetration area. Since defects penetrate along the migration direction, R_{eff} is also equal to R_s. In this way, the discrete diffusion mechanism will not change the effective radius R_{eff}, and the correction term $\Delta R = 0$.

3.1.3. Correction for high volume fraction sinks

The discrepancy at the high sink volume fraction region is likely a result of different sink configurations. In the OKMC simulation, sinks are randomly distributed in the simulation box and do not overlap with each other(non-overlap configuration). While in the theoretical model with the mean-field approximation, sinks are considered to be randomly and uniformly distributed in the system without taking care to avoid the overlapping between sinks (overlap configuration). In order to verify this speculation, we also constructed an overlap configuration in the OKMC simulation. The sink strengths under this configuration are calculated and their corresponding relative error is presented in Fig. 7. Compared with Fig. 4, the relative error becomes nearly zero throughout the considered range, which supports our hypothesis about the sink configurations.

The distinct behaviors between two configurations are likely to originate from the sink volume fractions. For the non-overlapping configuration, its volume fraction f_v is given by:

$$f_v = 4\pi R_s^3 N_s/3. \tag{9}$$

Due to the overlap between sinks, this formula does not apply to the overlap configuration. In the overlap configuration, a larger sink density $N_{s,lap} > N_s$

is required to occupy the same f_v to the non-overlap configuration. In this case, we define a dummy volume fraction that given by simply summing all sinks without caring about the overlap:

$$F_v = 4\pi R_s^3 N_{s,lap}/3. \tag{10}$$

The relationship between f_v and F_v is given by differential equations:

$$f_v(F_v + \mathrm{d}F_v) = f_v(F_v) + [1 - f_v(F_v)]\mathrm{d}F_v, \tag{11}$$

$$F_v\,(f_v = 0) = 0, \tag{12}$$

where $1 - f_v(F_v)$ represents the volume fraction of unoccupied regions. Solution of these two equations is:

$$F_v = \ln \frac{1}{1 - f_v}. \tag{13}$$

With this relationship, we find that the error function fits best with the relative error at the high volume fraction of Fig. 4(b) and Fig. 6(b) is given by:

$$e = \frac{F_v^4 - f_v^4}{f_v^4} = \frac{(\ln \frac{1}{1-f_v})^4 - f_v^4}{f_v^4}. \tag{14}$$

In the low volume fraction region, the probability of overlap is very low, and F_v is practically equal to f_v. Therefore, the relative error arising from the sink distribution is invisible. However, as the volume fraction increases, the overlap probability grows very rapidly. Therefore, the relative error becomes significantly large at the high volume fraction region. It should be pointed out that the overlap configuration is unrealistic in real materials, because F_v can exceed 100%. In order to handle the defect interaction under the high sink volume fractions, according to Eq. (14), the theoretical sink strengths need to be corrected by multiplying a coefficient $(\frac{\ln \frac{1}{1-f_v}}{f_v})^4$.

In addition, in the previous work of sink strength theory[1], Brailsford et al. pointed out an intrinsic part of their method is that the sample volume must be large compared with the inter-sink spacing in random arrays. This implies that the theoretical work is premised on the assumption of low sink volume fraction. Therefore, the additional correction for the high volume fraction sink should be reasonable.

3.1.4. Transition from 3D to 1D regime

The sink strength of spherical sinks for the mixed 1D/3D migration, $k^2_{1-3,s}$, can be described by a single-variable function [12] interpolating between the 1D and 3D limiting cases, i.e.,

$$y = \frac{1}{2}(1 + \sqrt{1 + 4/x^2}), \tag{15}$$

where y and x are two dimensionless variables. In the OKMC simulation, y and x are defined as:

$$y = k^2_{1-3,s}/k^2_{1,s}, \tag{16}$$

$$x = \frac{l^2_{ch}k^2_{1,s}}{12} + \frac{k^4_{1,s}}{k^4_{3,s}}, \tag{17}$$

where $l_{ch} = d\sqrt{\exp(E_r/k_BT)}$ is the average migration length between two direction changes.

In Fig. 8 (a), the simulated sink strengths of different densities of sinks under the mixed 1D/3D limit are plotted as a function of rotation the energy E_r. All simulations are conducted under the non-overlap configuration.Because we do not know the effective radius correction ΔR under this situation, the radius of sinks is chosen to be 4.25 nm, which is large enough to avoid the error introduced by effective radius change and also small enough to avoid the error from the overlap configuration. Sink density N_s varies from 3×10^{-5} to 1.5×10^{-4} nm^{-3}. As we can see, the sink strength smoothly transits from

3D to 1D migrating with the increasing E_r. And a rotation energy of 1.5 eV is high enough to ensure a pure 1D migration. The master-curve defined by Eq. (15) is illustrated in Fig. 8(b). Here we find that the analytical master-curve is in a perfect agreement with our simulated data.

3.2. Dislocation lines

According to the previous study [11], the theoretical sink strength of the 3D and 1D migration defects being absorbed by dislocation lines are [3, 4, 6]:

$$k_{3.d}^2 = \frac{2\pi\rho_d(1-\pi\rho_d R_d^2)}{0.25\pi\rho_d R_d^2(4-\pi\rho_d R_d^2) - 0.75 - \ln\left(R_d\sqrt{\pi\rho_d}\right)}, \tag{18}$$

and

$$k_{1.d}^2 = 6 \times (\pi R_d \rho_d)^2, \tag{19}$$

respectively. Here, R_d represents capture radius of the dislocation line, $\rho_d = l_z^{-2}$ is its surface density. Its volume fraction is given by $f_v = \pi R_d^2 \rho_d$.

3.2.1. 3D limit

Fig. 9(a) shows the sink strengths of dislocation lines under 3D migration limit. Similar to the situation of spherical sinks, a good agreement between simulation and theory is found but two discrepancies appear for dislocations with small R_d and with high volume fraction. The former discrepancy arises from the difference between diffusion mechanisms, which are continuous in the theory while discrete in the OKMC. This discrepancy can be well reconciled by introducing the effective radius correction to Eq. (18). The corrected equation is given by:

$$k_{3.d}^2 = \frac{2\pi\rho_d[1-\pi\rho_d(R_d+\Delta R)^2]}{\frac{1}{4}\pi\rho_d(R_d+\Delta R)^2[4-\pi\rho_d(R_d+\Delta R)^2] - \frac{3}{4} - \ln\left[(R_d+\Delta R)\sqrt{\pi\rho_d}\right]}. \tag{20}$$

Similar to Eq. (2), Eq. (18) is approximately a linear function of R_d when R_d is small. Therefore, the correction term ΔR should be similar to that

for spherical sinks. A detailed derivation of ΔR is a little bit tedious. For simplicity, we shall use the ΔR from Eq. (8)(simply replace R_s with R_d). As shown in Fig. 9(b), after the effective radius modification, the relative error in the low volume fraction region becomes nearly zero. On the other hand, the discrepancy at the high volume fraction cannot be explained as we discussed for the spherical sinks. This might be because that the analytical expression is based on an assumption that ρ_d is a small value, i.e., the low sink volume fraction. And the periodic boundary condition, which might cause an interplay between vicinal dislocations, is obviously not included in the theoretical model. Since such discrepancy is not obvious until the volume fraction is higher than 0.1, this is acceptable because the typical value in real materials is usually much smaller than 0.1.

3.2.2. 1D limit and the influence of the periodic configuration

Fig. 10 (a) and (b) show the sink strength and the relative error for dislocation lines under the 1D limit, grouped by dislocation surface densities. No effective radius correction is required here owing to the similar reason shown in the Fig. 5(b). The agreement between simulation and theory is less satisfactory than the 3D limit. Similar to the case of spherical sinks, a rapid growth of the relative error is also observed in the high volume fraction region, which can be described by Eq. (14). This indicates that the theoretical expression is also based on the overlap configuration. This significant error at the high volume fraction region can be eliminated by multiplying a coefficient $(\frac{\ln \frac{1}{1-f_v}}{f_v})^4$ to the right side of Eq. (19).

Figure. 10(c) shows the relative error after the correction. All data are positive and show a zigzag behavior as a function of the sink volume fraction. These positive errors may origin from a truncation of the tail of very long distance migration before absorption. Namely, in a completely

random distribution of dislocations, free migration distance of point defects before its absorption should follow an exponential distribution [6]:

$$P(L) = \pi R_d \rho_d \exp(-\pi R_d \rho_d L), \tag{21}$$

where L is the free migration distance and $P(L)$ is its probability density. Any positive L can be achieved with a positive probability density in such configuration. However, in a periodic dislocation configuration, such very long distance migrations are cut out. Fig. 11 shows a sketch of this cut-tail effect. In a periodically extended simulation box, 1D migration defects cannot travel to a distance longer than L_{cut1}. Meanwhile, we also find that the cutoff distance L_{cut} does not vary continuously with R_d. A slight reduction of the dislocation radius from R_{d1} to R_{d2} might cause a mutation of the cutoff distance (L_{cut1} to L_{cut2}). Such cut-tail effect will reduce the average migration distance, which consequently causes an overestimate of the theoretical sink strength. Therefore, the mutation of the cutoff distance is responsible for the zigzag behavior of relative errors.

Figure 12(a) shows the cutoff distance in OKMC, L_{cut}, as a function of the sink volume fraction. The average migration distance, $\overline{L} = (\pi R_d \rho_d)^{-1}$ [6], calculated from Eq. (21) is also plotted for comparisons. With an increase of the volume fraction, the cutoff distance decreases step by step like a staircase. The ratio of L_{cut} to $\overline{L}$ is shown in Fig. 12(b). Four high peaks and four low peaks can be clearly distinguished here. Each of them represents a mutation of the cutoff distance. The high peaks in Fig. 12(b) correspond to four main peaks of relative error in Fig. 10(c) (labeled with green vertical lines), while the low peaks correspond to four shoulder peaks of relative error in Fig. 10(c) (blue vertical lines). Although we are aware of the origin of these error peaks, it is still very difficult to build a complete random configuration to eliminate them. More studies are required in the future to achieve a

consistency between theory and OKMC simulation.

Note that, our results are different from the previous work by Jansson et al. [11], where the relative error tends to be negative in the low volume fractions, but positive in the high volume fraction region. This difference is likely contributed to the different simulation box we used. In our work, the ratio of box sides perpendicular to the dislocation is an irrational number, $l_x : l_y = \sqrt{2}$. While in the previous simulation, the ratios are rational numbers. It has been pointed out [10] that in order to prevent endless migrations of 1D point defects, a non-cubic (non-square in this situation) box is instrumental to simulate correctly the 1D migrating defects. However, a box with a rational ratio, for instance $l_x : l_y = 400a_0 : 350a_0$, is equally a square super-box with $L_x : L_y = 7l_x : 8l_y = 2800a_0 : 2800a_0$. The square super-box cannot completely prevent the endless migrations from happening in low sink volume fraction region. Once an endless migration is started, the point defect cannot be absorbed until the simulation is halted manually. This should be restrictively forbidden because it would increase the free migration distance unpredictively, and lead to a negative relative error in the low volume fraction region.

3.2.3. Transition from 3D to 1D regime

The transition between 3D migrating and 1D migrating is illustrated in Fig. 13(a). The capture radii were carefully chosen to ensure the volume fraction $f_v = 0.005$ and $f_v = 0.03$. Because the simulation results fit very well with the theory for both 3D and 1D migrating at these volume fractions. The transition is more abrupt compared to the simulation of spherical sinks. The 1D regime is already reached at $E_r = 1.0$ eV. Meanwhile, in the master-curve representation (Fig. 13(b)), the simulation always gives a lower value than the analytical one in the 3D migrating region. This was also found

in the previous study [11]. However, unlike their results, we find that the simulation data of the same volume fraction collapse onto the same curve, which indicates that the volume fraction should be the key variable of this discrepancy.

4. Conclusion

We performed a series of OKMC simulations to study the sink strengths of spherical sinks and dislocation lines with different radii and volume fractions. The simulation results were compared with the theoretical expressions derived from diffusion theory to evaluate the validity of these expressions, and further, to modify these expressions.

For the small sinks, the discrepancy between the diffusion theory and simulation is caused by the different migration distances used in these two methods. This can be resolved by adding a correction term to the effective radius of sinks. For the high volume fraction sinks, the discrepancy is attributed to different sink configurations in two methods. It can be eliminated by introducing a compensation term of sink volume fraction to the theoretical expressions. For dislocation lines under the 1D migration limit, a zigzag like discrepancy is found. It is caused by the periodic distribution of dislocation lines adopted in OKMC.

Based on these results, the origins of the above discrepancies have been revealed and successfully resolved. This can extend the capability of mean-field approaches to properly reproduce the defect evolution of irradiated materials, and provide a better insight into experimental phenomena, such as the defect cluster, the irradiation-induced swelling and the blistering.

Acknowledgement

This work was supported by the National Magnetic Confinement Fusion Program (Grant No.: 2015GB112001), the National Natural Science Foundation of China (Nos.: 11505229, 11575229, 11375231), the Youth Innovation Promotion Association of CAS (2015384), and by the Center for Computation Science, Hefei Institutes of Physical Sciences.

[1] A. D. Brailsford, R. Bullough, Philos. Trans. R. Soc. London. 302 (1981) 87 - 137.

[2] R. Bullough, M. R. Hayns, M. H. Wood, J. Nucl. Mater. 90 (1980) 44 - 59.

[3] H. Wiedersich, Radiat. Eff. 12 (1972) 111 - 125.

[4] F. A. Nichols, J. Nucl. Mater. 75 (1978) 32 - 41.

[5] H. Rouchette, L. Thuinet, A. Legris, A. Ambard, C. Domain, Comput. Mater. Sci. 88 (2014) 50 - 60.

[6] A. V. Brarshev, S. I. Golubov, H. Trinkaus, Philos. Mag. A 81 (2001) 2515 - 2532.

[7] M. J. Caturla, N. Soneda, E. Alonso, B. D. Wirth, T. Díaz de la Rubia, J. M. Perlado, J. Nucl. Mater. 276 (2000) 13 - 21.

[8] N. Soneda, S. Ishino, A. Takahasi, K. Dohi, J. Nucl. Mater. 323 (2003) 169 - 180.

[9] C. Domain, C.S. Becquart, L. Malerba, J. Nucl. Mater. 335 (2004) 121 - 145.

[10] L. Malerba, C. S. Becquart, C. Domain, J. Nucl. Mater. 360 (2007) 159 - 169.

[11] V. Jansson, L. Malerba, A. De Backer, C. S. Becquart, C. Domain, J. Nucl. Mater. 442 (2013) 218 - 226.

[12] H. Trinkaus, H. L. Heinisch, A. V. Barashev, S. I. Golubov, B. N. Singh, Phys. Rev. B 66 (2002) 060105.

[13] H. L. Heinisch, B. N. Singh, S. I. Golubov, J. Nucl. Mater. 283 - 287 (2000) 737 - 740.

[14] H. L. Heinisch, B. N. Singh, Philos. Mag. 83 (31 - 34) (2003) 3661 - 3676.

[15] H. L. Heinisch, H. Trinkaus, B. N. Singh, J. Nucl. Mater. 367 - 370 (2007) 332 - 337.

[16] R. E. Stoller, S. I. Golubov, C. Domain, C. S. Becquart, J. Nucl. Mater. 382 (2008) 77 - 90.

[17] W. Young, E. Elcock, Proc. Phys. Soc. 89 (1966) 735.

[18] R. Panvani, G. Ranchino, Comput. Chem. 6 (1982) 133 - 135.

Figure caption:

Figure 1 Schematic of the non-cubic box and the dislocation line model in OKMC. The periodic boundary condition is applied in all three dimensions.

Figure 2(color online) The first to the fifth iterative order approximation of Eq. (2). Here, the largest sink radius of our simulations, $R_s = 10.25$ nm, is used for convergence test. The sink volume fraction is given by $f_v = 4\pi R_s^3 N_s/3$, where N_s is the number density of spherical sinks.

Figure 3(color online) Sink strength of spherical sinks with different radii versus sink volume fraction, lines are results of Eq. (2) and Eq. (3), dots are the corresponding simulated results. (a) and (b) represents 3D migration and 1D migration limit, respectively.

Figure 4(color online) The relative error between theoretical and simulated sink strength that presented in Fig. 3. (a) and (b) represents 3D migration and 1D migration limit, respectively. The solid line represents the error estimated by Eq. (14).

Figure 5(color online) Schematics of a point defect being absorbed by a spherical sink under two different diffusion mechanisms. The gray area represents the penetration area in OKMC simulation. (a) 3D migration limit. The effective radius, R_{eff}, is the weighted average of the penetration depth p. Shadow area represents possible start points those can jump into the segment from r to $r + \mathrm{d}r$; (b) 1D migration limit. R_{eff} is the radius of the biggest cross-section perpendicular to the migration direction of the penetration area, which equals sink radius R_s in this case.

Figure 6(color online) Results of 3D migration defects absorbed by spherical sinks with different radii, theoretical values are calculated by Eq. (4) with ΔR from Eq. (8). (a) sink strength from simulation (dots) and the theoretical expression (lines). (b) the relative error between simulation and the theoretical expression, solid line represents the error estimated by Eq. (14).

Figure 7(color online) The relative error between theoretical (by Eq. (4) with ΔR from Eq. (8), and by Eq. (3)) and simulated sink strength of spherical sinks, under a configuration that sinks are allowed to overlap without any reaction takes place. (a) and (b) represents 3D migration and 1D migration limits, respectively.

Figure 8(color online) The transition from 3D to 1D migration limit for 4.25 nm spherical sinks, grouped by sink densities. (a) simulated sink strength as a function of rotation energy, with temperature $T = 723$ K. (b) the master-curve representation, the solid line represents the theoretical relationship of x and y in Eq. (15), dots are the simulation results elaborated according to Eqs. (16) and (17).

Figure 9(color online) Results of 3D migration defects absorbed by dislocation lines, grouped by box sizes with a fixed ratio. (a) sink strength from simulation (empty dots) and theoretical expression (dotted and solid lines are the results from Eqs. (18) and (20), respectively). (b) the relative error between simulation and theoretical expression (empty and solid dots are the results using Eqs. (18) and (20), respectively).

Figure 10(color online) Results of 1D migration defects absorbed by dislocation lines, grouped by box sizes with a fixed ratio. (a) sink strength from simulation (empty dots) and theoretical expression (solid lines). (b) the relative error between simulation and theoretical expression, the solid line represents the error estimated by Eq. (14). (c) data obtained by removing the error described by Eq. (14) from (b). Vertical lines are the corresponding position of mutation peaks in Fig. 12(b).

Figure 11(color online) Schematics of 1D migration in a periodically extended simulation box in OKMC, picture is taken perpendicular to the direction of dislocation lines. Two kinds of round circles represent dislocation lines with different radii. The furthest migration distance, namely the cutoff distance, is labeled by L_{cut1} and L_{cut2}. Dislocations with radius R_{d1} (left) corresponding to a cutoff distance of L_{cut1}, while a slightly reduction of the dislocation radius from R_{d1} to R_{d2} (right) will cause a mutation of the cutoff distance from L_{cut1} to L_{cut2}.

Figure 12(color online) (a) the mutation of the cutoff distance (in the unit of box size l_z), L_{cut}, of 1D migration as the function of volume fraction, compared with the average migration distance, $\overline{L}$, obtained from Eq. (21). (b) the ratio of L_{cut} to $\overline{L}$, each peak represents a mutation of the cutoff distance. Four high peaks corresponding to the four main peaks of relative error in Fig. 10(c), while the four lower peaks corresponding to four shoulder peaks of relative error in Fig. 10(c).

Figure 13(color online) The transition from 3D to 1D migrating sink strength of point defects absorbed by dislocation lines, grouped by box sizes, where the volume fraction of sinks is fixed at $f_v = 0.005$ and $f_v = 0.03$ (denoted by empty and solid dots, respectively). (a) simulated sink strength as a function of rotation energy, with temperature $T = 723$ K. (b) the master-curve representation, solid line represents the theoretical relationship of x and y in Eq. (15), dots are the simulation results elaborated according to Eqs. (16) and (17).

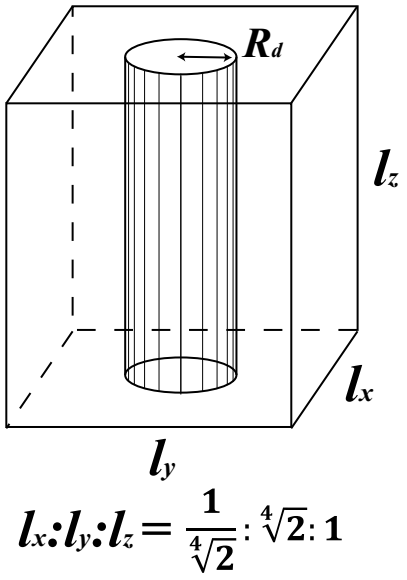

Figure 1: Schematic of the non-cubic box and the dislocation line model in OKMC. The periodic boundary condition is applied in all three dimensions.

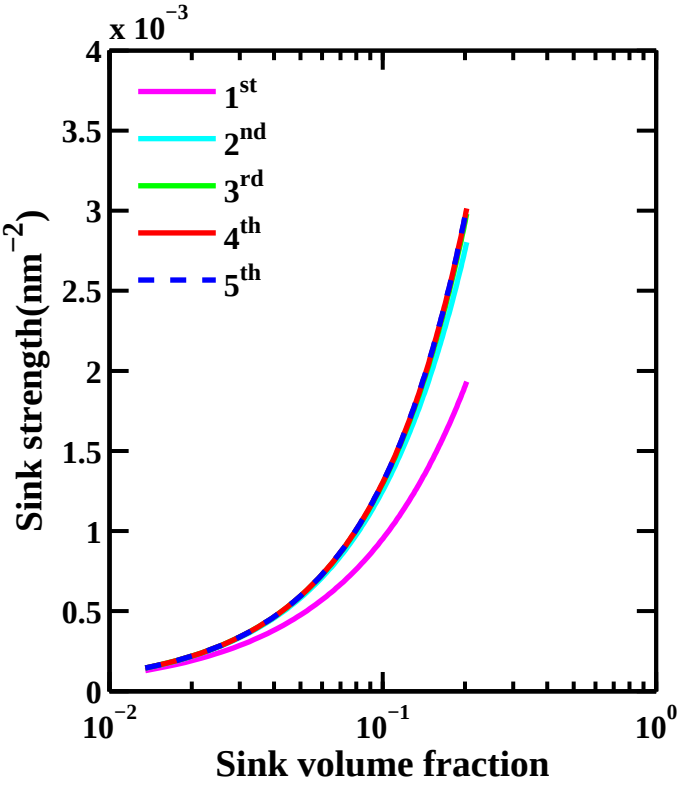

Figure 2: (color online) The first to the fifth iterative order approximation for sink strength from Eq. (2). Here, the largest sink radius of our simulations, $R_s = 10.25$ nm, is used for convergence test. The sink volume fraction is given by $f_v = 4\pi R_s^3 N_s/3$, where N_s is the number density of spherical sinks.

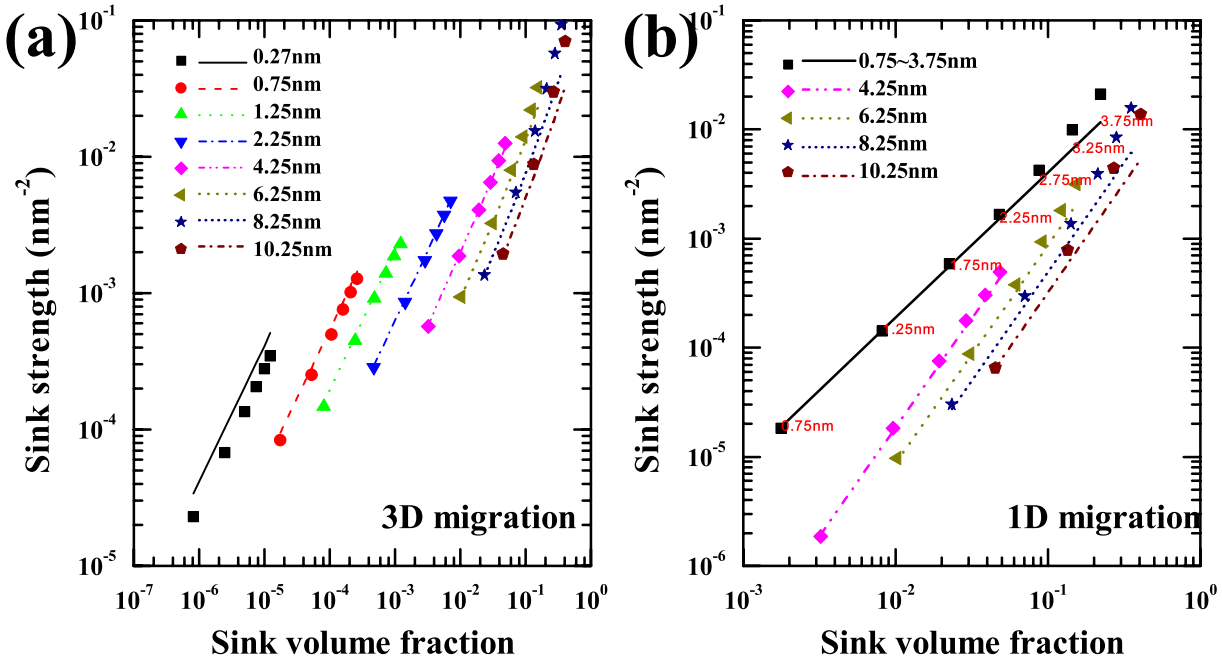

Figure 3: (color online) Sink strength of spherical sinks with different radii versus sink volume fraction, lines are results of Eq. (2) and Eq. (3), dots are the corresponding simulated results. (a) and (b) represents 3D migration and 1D migration limit, respectively.

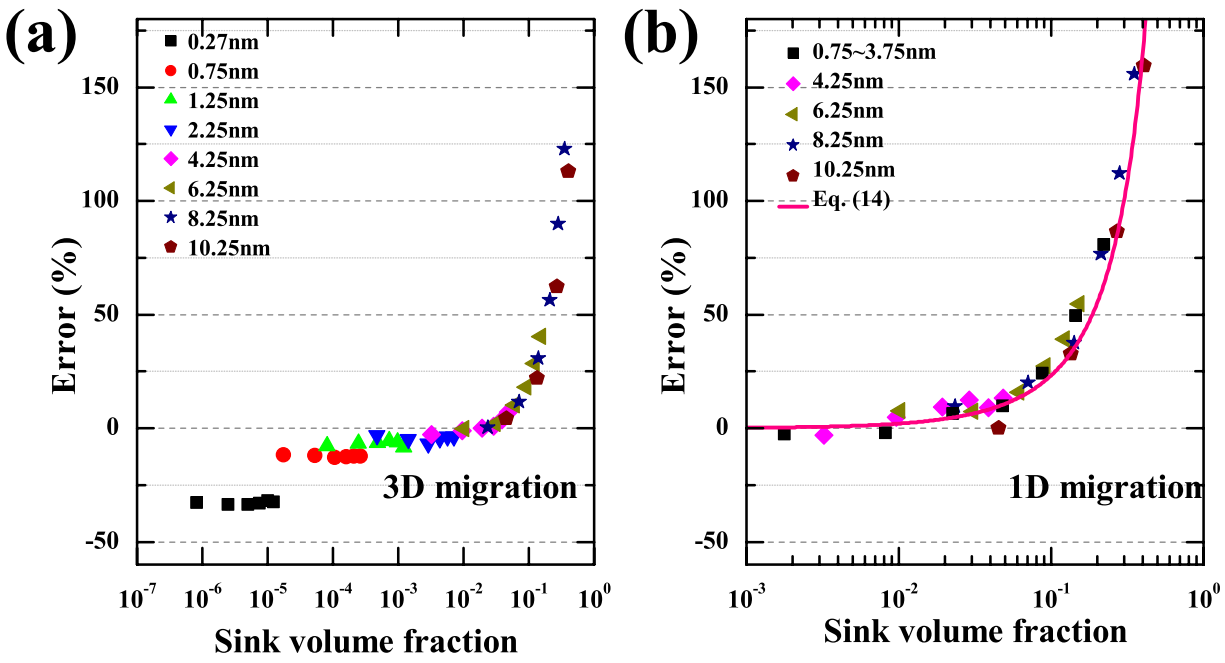

Figure 4: (color online) The relative error between theoretical and simulated sink strength that presented in Fig. 3. (a) and (b) represents 3D migration and 1D migration limit, respectively. The solid line represents the error estimated by Eq. (14).

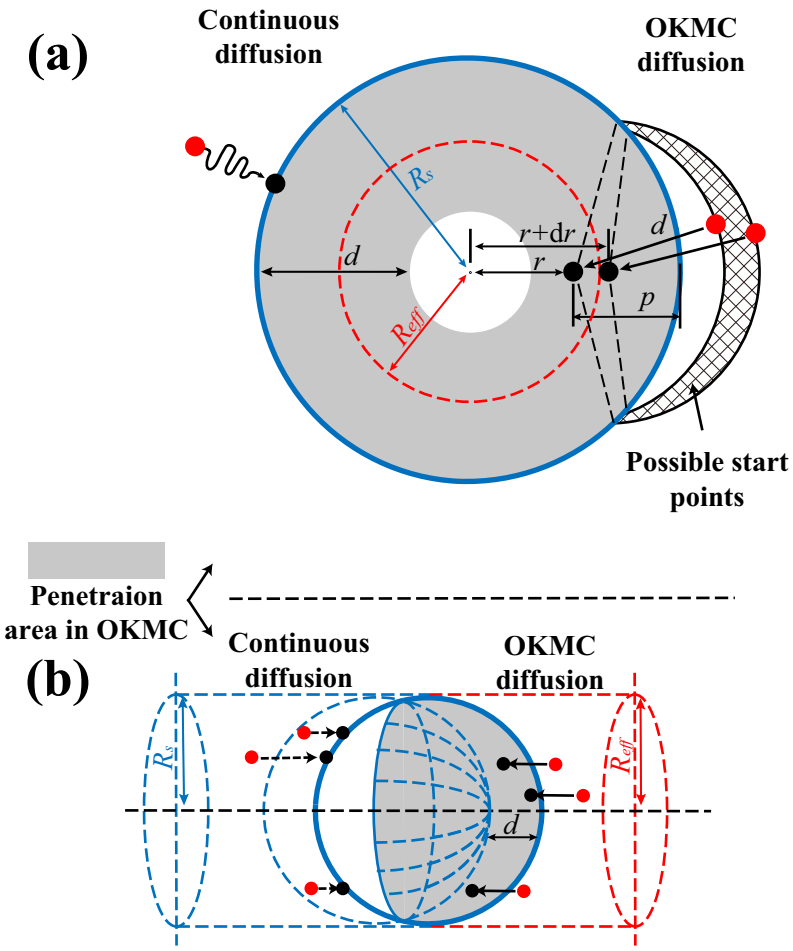

Figure 5: (color online) Schematics of a point defect being absorbed by a spherical sink under two different diffusion mechanisms. The gray area represents the penetration area in OKMC simulation. (a) 3D migration limit. The effective radius, R_{eff}, is the weighted average of the penetration depth p. Shadow area represents possible start points those can jump into the segment from r to $r + \mathrm{d}r$; (b) 1D migration limit. R_{eff} is the radius of the biggest cross-section perpendicular to the migration direction of the penetration area, which equals sink radius R_s in this case.

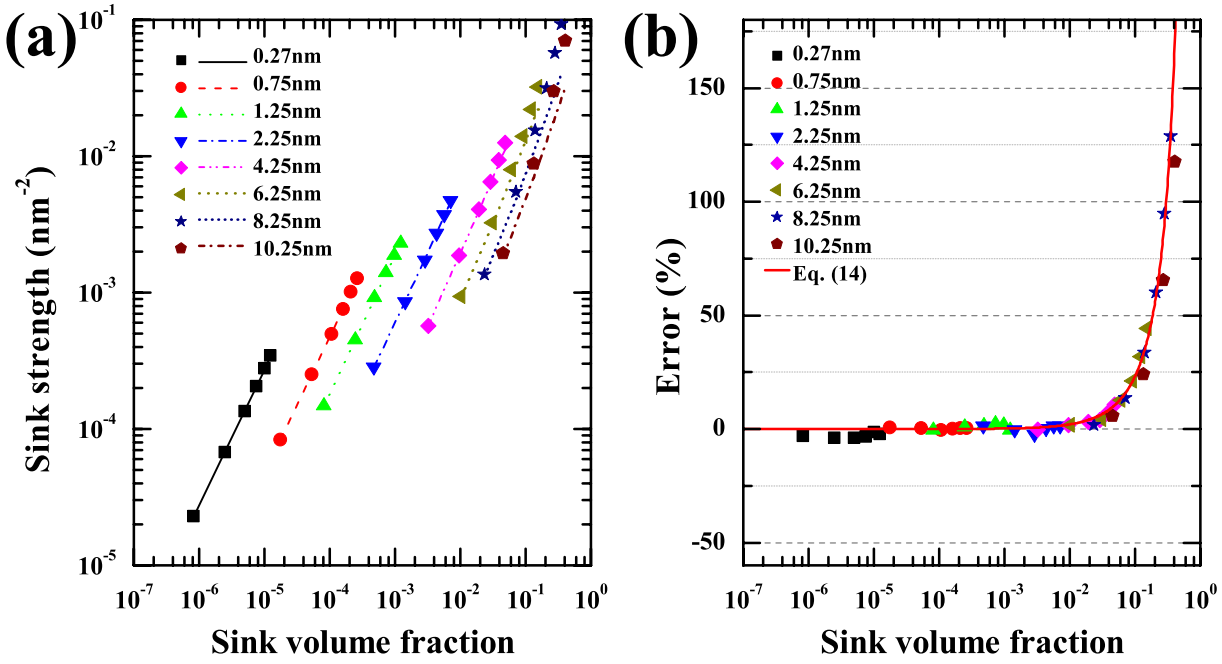

Figure 6: (color online) Results of 3D migration defects absorbed by spherical sinks with different radii, theoretical values are calculated by Eq. (4) with ΔR from Eq. (8). (a) sink strength from simulation (dots) and the theoretical expression (lines). (b) the relative error between simulation and the theoretical expression, solid line represents the error estimated by Eq. (14).

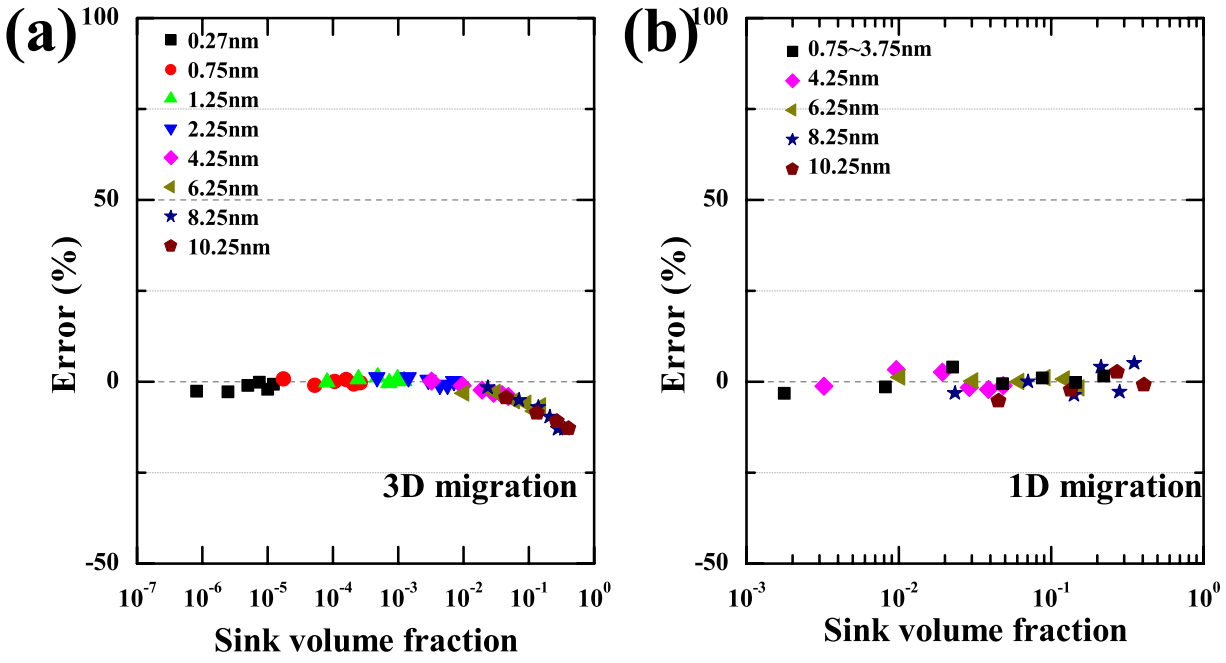

Figure 7: (color online) The relative error between theoretical (by Eq. (4) with ΔR from Eq. (8), and by Eq. (3)) and simulated sink strength of spherical sinks, under a configuration that sinks are allowed to overlap without any reaction takes place. (a) and (b) represents 3D migration and 1D migration limits, respectively.

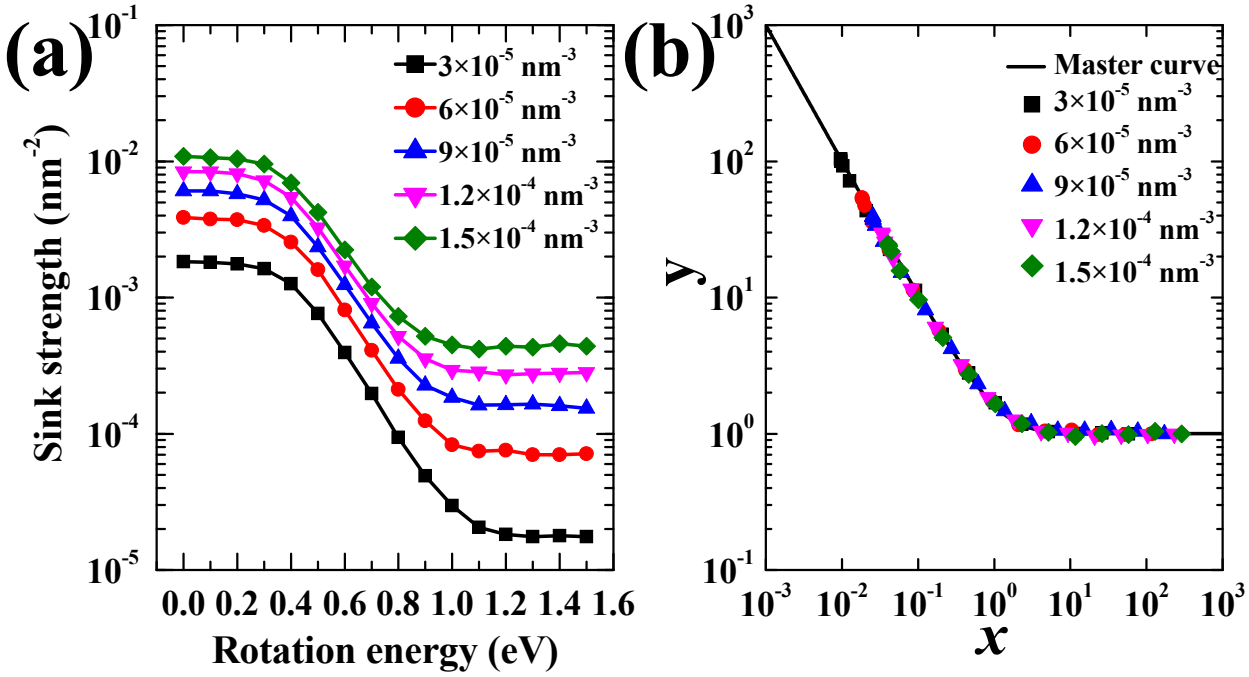

Figure 8: (color online) The transition from 3D to 1D migration limit for 4.25 nm spherical sinks, grouped by sink densities. (a) simulated sink strength as a function of rotation energy, with temperature $T = 723$ K. (b) the master-curve representation, the solid line represents the theoretical relationship of x and y in Eq. (15), dots are the simulation results elaborated according to Eqs. (16) and (17).

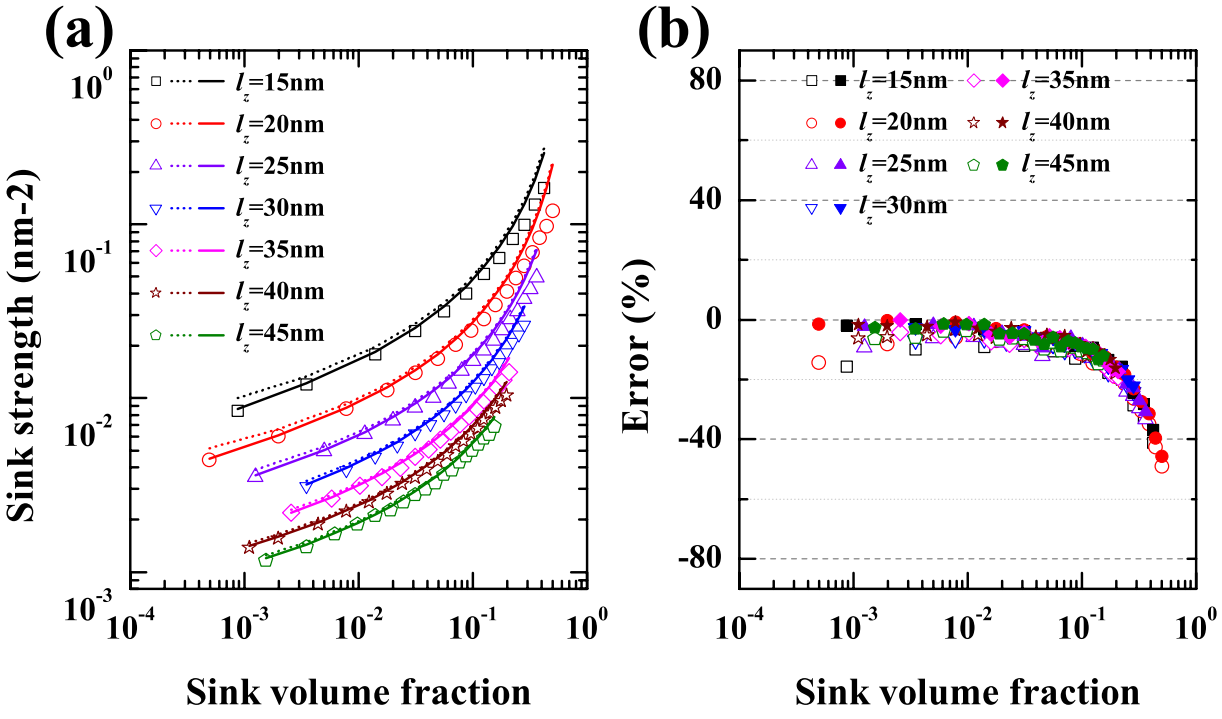

Figure 9: (color online) Results of 3D migration defects absorbed by dislocation lines, grouped by box sizes with a fixed ratio. (a) sink strength from simulation (empty dots) and theoretical expression (dotted and solid lines are the results from Eqs. (18) and (20), respectively). (b) the relative error between simulation and theoretical expression (empty and solid dots are the results using Eqs. (18) and (20), respectively).

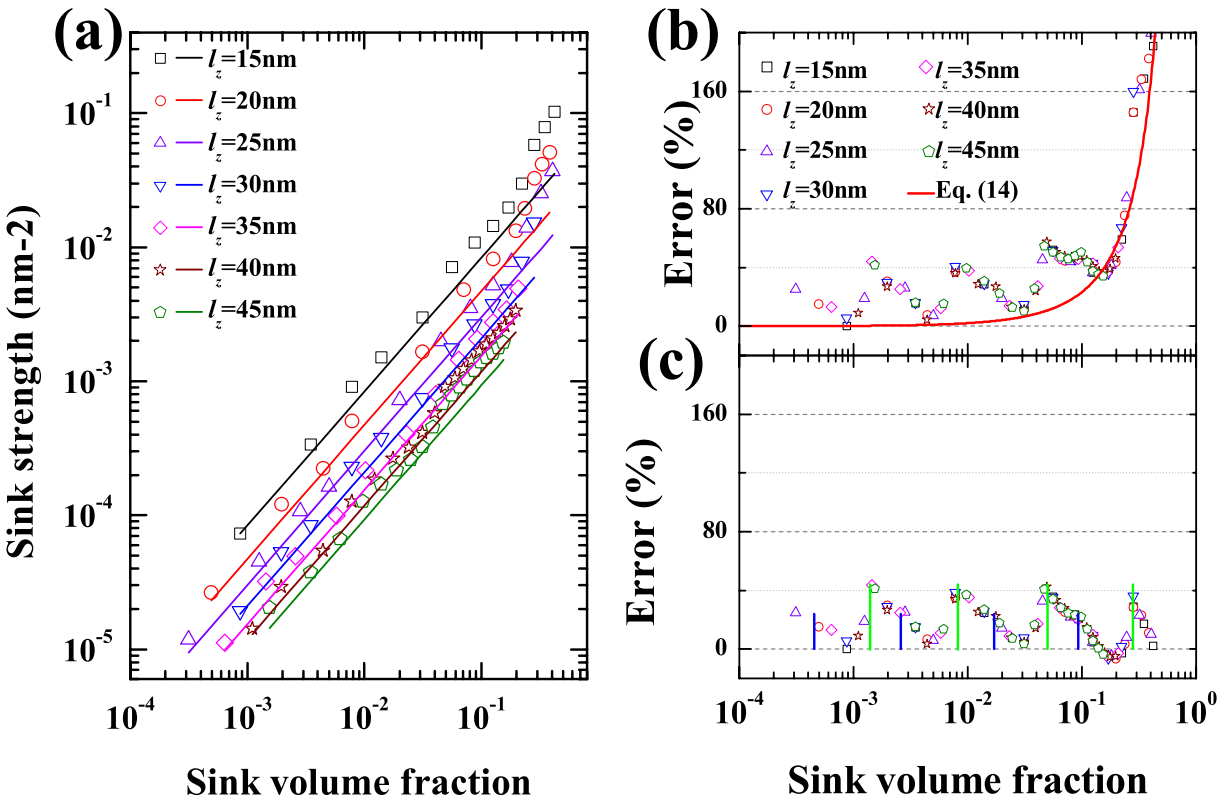

Figure 10: (color online) Results of 1D migration defects absorbed by dislocation lines, grouped by box sizes with a fixed ratio. (a) sink strength from simulation (empty dots) and theoretical expression (solid lines). (b) the relative error between simulation and theoretical expression, the solid line represents the error estimated by Eq. (14). (c) data obtained by removing the error described by Eq. (14) from (b). Vertical lines are the corresponding position of mutation peaks in Fig. 12(b).

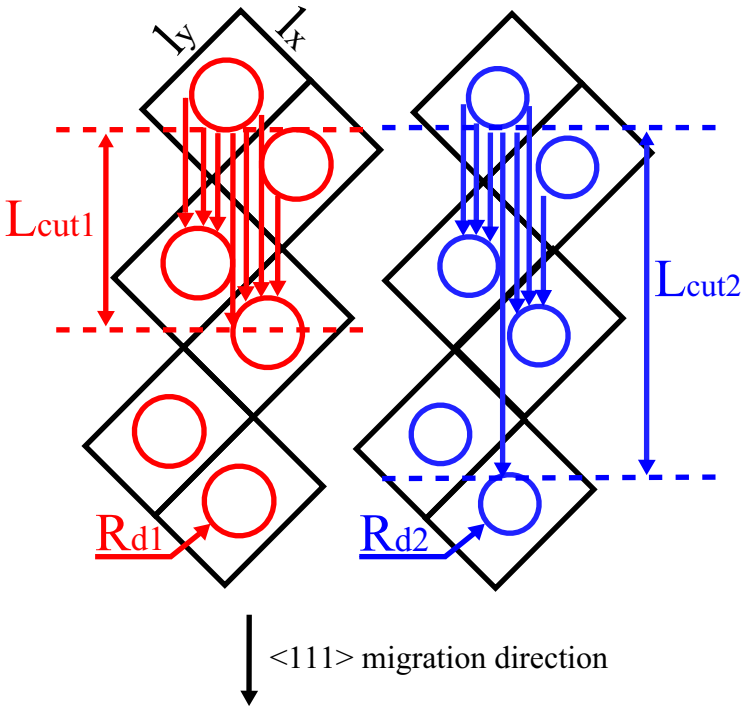

Figure 11: (color online) Schematics of 1D migration in a periodically extended simulation box in OKMC, picture is taken perpendicular to the direction of dislocation lines. Two kinds of round circles represent dislocation lines with different radii. The furthest migration distance, namely the cutoff distance, is labeled by L_{cut1} and L_{cut2}. Dislocations with radius R_{d1} (left) corresponding to a cutoff distance of L_{cut1}, while a slightly reduction of the dislocation radius from R_{d1} to R_{d2} (right) will cause a mutation of the cutoff distance from L_{cut1} to L_{cut2}.

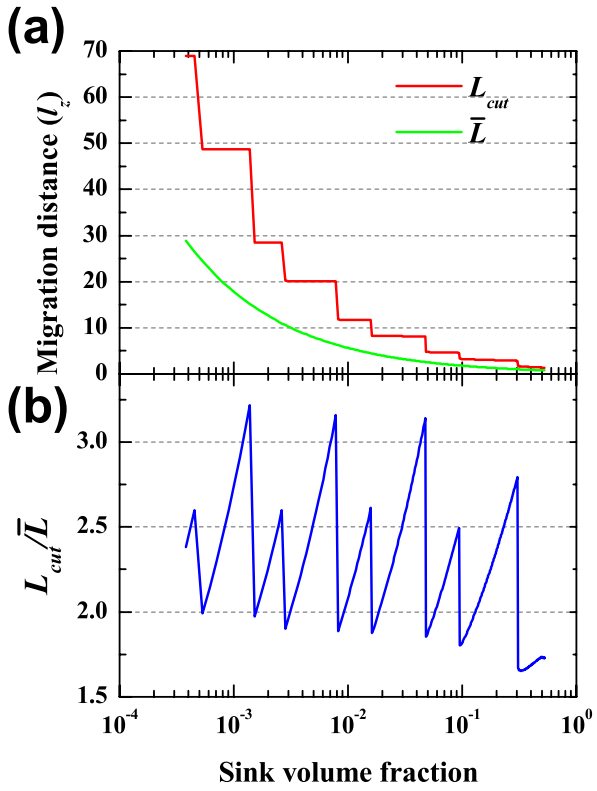

Figure 12: (color online) (a) the mutation of the cutoff distance (in the unit of box size l_z), L_{cut}, of 1D migration as the function of volume fraction, compared with the average migration distance, $\overline{L}$, obtained from Eq. (21). (b) the ratio of L_{cut} to $\overline{L}$, each peak represents a mutation of the cutoff distance. Four high peaks corresponding to the four main peaks of relative error in Fig. 10(c), while the four lower peaks corresponding to four shoulder peaks of relative error in Fig. 10(c).

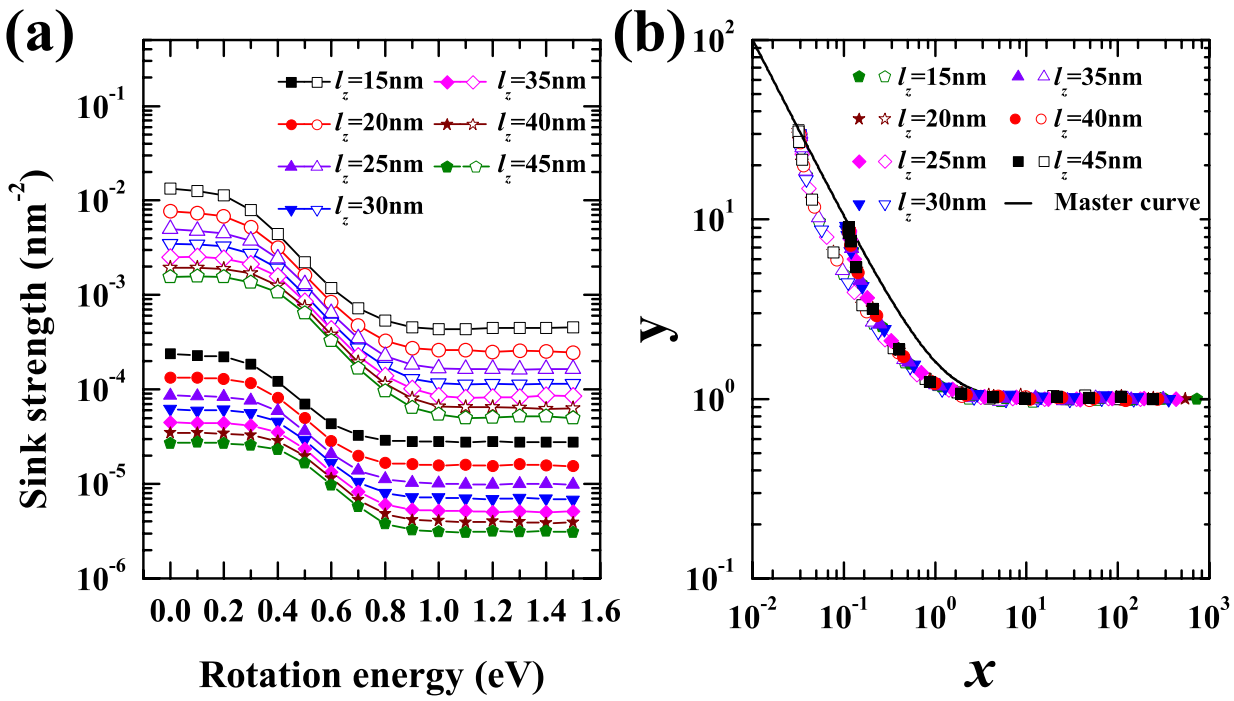

Figure 13: (color online) The transition from 3D to 1D migrating sink strength of point defects absorbed by dislocation lines, grouped by box sizes, where the volume fraction of sinks is fixed at $f_v = 0.005$ and $f_v = 0.03$ (denoted by empty and solid dots, respectively). (a) simulated sink strength as a function of rotation energy, with temperature $T = 723$ K. (b) the master-curve representation, solid line represents the theoretical relationship of x and y in Eq. (15), dots are the simulation results elaborated according to Eqs. (16) and (17).